

Adversarial Patch Generation for Visual-Infrared Dense Prediction Tasks via Joint Position-Color Optimization

He Li, Wenyue He, Weihang Kong, Xingchen Zhang*, *Member, IEEE*

Abstract—Multimodal adversarial attacks for dense prediction remain largely underexplored. In particular, visual-infrared (VI) perception systems introduce unique challenges due to heterogeneous spectral characteristics and modality-specific intensity distributions. Existing adversarial patch methods are primarily designed for single-modal inputs and fail to account for cross-spectral inconsistencies, leading to reduced attack effectiveness and poor stealthiness when applied to VI dense prediction models. To address these challenges, we propose a joint position-color optimization framework (AP-PCO) for generating adversarial patches in visual-infrared settings. The proposed method optimizes patch placement and color composition simultaneously using a fitness function derived from model outputs, enabling a single patch to perturb both visible and infrared modalities. To further bridge spectral discrepancies, we introduce a cross-modal color adaptation strategy that constrains patch appearance according to infrared grayscale characteristics while maintaining strong perturbations in the visible domain, thereby reducing cross-spectral saliency. The optimization procedure operates without requiring internal model information, supporting flexible black-box attacks. Extensive experiments on visual-infrared dense prediction tasks demonstrate that the proposed AP-PCO achieves consistently strong attack performance across multiple architectures, providing a practical benchmark for robustness evaluation in VI perception systems.

Index Terms—Adversarial patches, Multimodal attacks, Joint optimization, Visible-infrared fusion

I. INTRODUCTION

DEEP learning models have achieved remarkable success in a wide range of visual perception tasks and image processing [1]–[3]. However, despite their strong performance, these models remain vulnerable to adversarial perturbations, making security a growing concern in computer vision [4], [5]. This motivates systematic investigation of the vulnerability of modern perception systems under adversarial perturbations, especially in safety-critical settings.

Visual-infrared (VI) perception has become increasingly important because the two modalities provide complementary

This paper was supported partly by the National Natural Science Foundation of China (No. 62306264, 62173290), the Central Government Guided Local Funds for Science and Technology Development of China (No. 236Z0303G), the Natural Science Foundation of Hebei Province in China (No. F2024203091, F2025203045), Innovation Capability Improvement Plan Project of Hebei Province, China (No. 22567626H), the Royal Society Research Grant (No. RG\R1\251462), the Royal Society-NSFC International Exchanges Grant (No. W2521174) and Yanshan University (No. 2025LGGH003).

Weihang Kong, Wenyue He, and He Li are with the School of Artificial Intelligence (School of Software), Yanshan University, Qinhuangdao 066004, China. (Email: whkong@ysu.edu.cn; hewenyue@stumail.yisu.edu.cn; lihe@ysu.edu.cn)

Xingchen Zhang is with the Fusion Intelligence Laboratory, Department of Computer Science, University of Exeter, EX4 4RN, United Kingdom. (Email: x.zhang12@exeter.ac.uk)

* Corresponding author: Xingchen Zhang

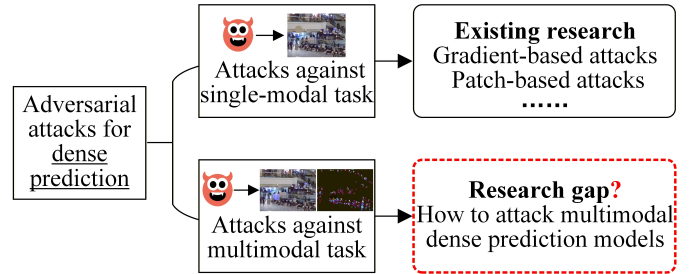


Fig. 1. Comparison of existing adversarial attack work and this study. The security of visual-infrared dense prediction models, remains underexplored compared with single-modal settings. This study aims to fill this gap.

cues: visible images capture rich texture and color, while infrared images remain informative under low illumination and adverse weather. This complementarity has motivated broad adoption of VI data in dense prediction tasks, such as crowd counting [6], semantic segmentation [7], and image fusion [8], under diverse environmental conditions.

Despite this growing use, the security and robustness of VI dense prediction models remain far less studied than their single-modal counterparts, leaving an important yet underexplored dimension of multimodal perception security. As illustrated in Fig. 1, existing adversarial research has predominantly concentrated on single-modal settings, with limited attention paid to VI dense prediction scenarios.

As a consequence, most existing adversarial attacks are developed under single-modal assumptions, primarily focusing on visible images [9], [10]. When directly applied to VI dense prediction tasks, these methods often exhibit degraded effectiveness due to substantial spectral differences between visible and infrared inputs. Dense prediction further increases the difficulty of attack design because model responses are spatially distributed over dense outputs. Consequently, adversarial patterns effective in the visible domain may not reliably transfer to VI dense prediction models. Among various attack forms, adversarial patches are especially relevant because they are physically realizable and offer a flexible carrier for modality-aware perturbation design [11]. Their effectiveness mainly depends on two factors: spatial deployment (position and coverage) and spectral appearance design (e.g., color/texture). Jointly optimizing these two factors is critical for achieving strong yet stealthy attacks, especially in VI dense prediction where spatial placement and appearance jointly influence pixel-level responses. Although several studies attempt joint optimization [12], [13], most of them still treat spatial and content updates in loosely coupled or sequential manners, leading to limited generalization in VI dense prediction settings.

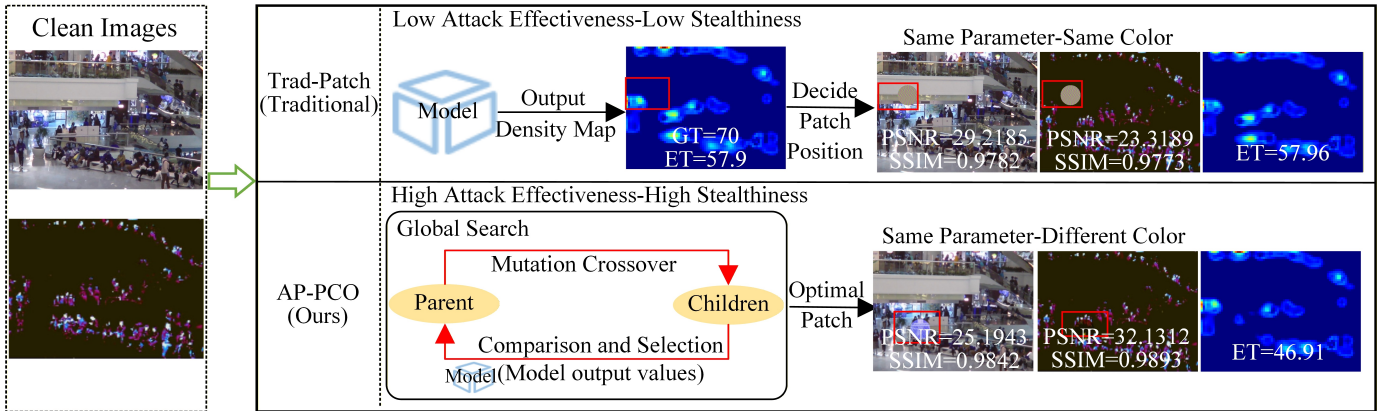


Fig. 2. Comparison between traditional adversarial patches (“Trad-Patch”) and the proposed patch (“AP-PCO”). Traditional methods determine the patch position based on a single forward pass of the target model and do not optimize color for multimodal data, which limits their effectiveness and stealthiness in visual–infrared settings. In contrast, our approach performs iterative, gradient-free global search to jointly determine position and color, and incorporates a cross-modal color reuse strategy to achieve stronger attacks and better stealthiness.

For position optimization, most existing works rely heavily on task-specific information (e.g., bounding boxes in object detection or density peaks in crowd counting), which does not generalize to dense prediction models without explicit region proposals. This lack of transferable cues makes it difficult to locate effective attack regions, especially in heterogeneous visual–infrared settings, as shown in Fig. 2.

Regarding content optimization, many existing methods rely on GAN-based iterative strategies [14]. These methods need large-scale training data to learn content distributions and generation mappings, entailing complex training. Existing techniques mainly include texture-based [12], [15] and color-based optimization [13]. Texture methods can generate complex patterns but become inefficient and unstable in visual–infrared settings because of the fundamental differences between the modalities. Color optimization is more efficient, as it avoids modeling fine-grained structures, but current color-mapping designs do not adapt across modalities: patches optimized for visible images often fail to transfer to infrared images and produce noticeable artifacts (Fig. 2), making it difficult to balance attack strength and stealthiness.

Furthermore, although some methods attempt joint optimization, spatial and appearance updates are typically implemented in sequential or loosely coupled manners, limiting effective coordination between the two factors. Such weak coupling is particularly problematic for visual–infrared dense prediction, where spatial placement and appearance jointly influence pixel-level model responses.

In addition, adversarial patches are parameterized by a mixed discrete–continuous structure: spatial parameters determine a binary mask, while color parameters define continuous perturbations within the selected region. This mixed parameterization further complicates the optimization landscape in cross-modal settings, making effective joint perturbation design inherently challenging.

To address these challenges, we propose a global search mechanism that jointly optimizes patch position and color via simulating population evolution in a high-dimensional solution space. This mechanism reduces reliance on task and

model-specific cues and achieves better generalization across visual–infrared dense prediction tasks by avoiding separate mismatched optimization. Additionally, we present a cross-modal color reuse strategy (mask multiplication, grayscale compression, background superposition) to resolve infrared image artifacts (Fig. 2). It ensures cross-modal color consistency, enables the patch to naturally integrate with infrared grayscale characteristics while maintaining high brightness in visible images, and balances attack strength with stealthiness.

The main contributions of this paper are as follows:

- We formulate VI dense prediction patch attacks as a joint spatial-spectral optimization problem and propose a population-based global search mechanism to jointly optimize patch position and color for visible and infrared inputs, achieving consistent attack performance across different models and tasks.
- We introduce a cross-modal color parameter reuse strategy that adapts a shared appearance representation to both visible and infrared modalities, effectively reducing infrared saliency while maintaining strong perturbations in the visible domain.
- We conduct comprehensive experiments on three representative VI dense prediction tasks (i.e., crowd counting, semantic segmentation, and image fusion) and evaluate the proposed method under multiple defense strategies. The results demonstrate consistent attack effectiveness across diverse architectures, tasks, and defense settings.

II. RELATED WORK

A. Visual-infrared perception

Visible and infrared images have been widely applied in perception tasks such as crowd counting [6], semantic segmentation [7], and image fusion [8]. Their complementary sensing properties, where visible images capture detailed textures and infrared images provide stable thermal information under low illumination, make visual–infrared perception systems essential for all-weather computer vision. However, the multimodal nature of these systems also presents unique challenges for AI

security because perturbations may affect visible and infrared representations in different ways.

Despite the growing importance of visual–infrared perception, very few studies have examined adversarial attacks in this setting. The robustness of multimodal perception models therefore remains insufficiently understood, leaving a clear gap for systematic investigation.

B. Adversarial attacks

Adversarial attacks aim to mislead a trained model during inference by introducing carefully crafted perturbations to the input data [16]. Depending on the attacker’s knowledge of the target model, attacks are typically categorized into white-box and black-box settings. White-box attacks [17] assume full access to model parameters and gradients, while black-box attacks [18] rely on query-based optimization or transferability without requiring internal model information.

From the implementation perspective, attacks can occur in the digital domain [19], [20] or the physical domain [21], [22]. Adversarial patches form an important bridge between the two, as they can be optimized digitally and deployed physically with high practicality. Brown et al. [23] first introduced adversarial patches for single-modal image recognition, leading to a series of patch-based methods for visible images, such as APAM [24] and PAP [10]. Sun et al. [25] further demonstrated that local patch manipulation can significantly degrade image fusion models. However, all these approaches operate exclusively in the visible modality.

Research on adversarial attacks for VI dense prediction remains extremely limited. The perception fusion framework [26] employs PGD to generate adversarial samples, but relies on gradients and does not support patch-based physical deployment. Motivated by this gap, this work focuses on visual–infrared cross-modal tasks and aims to design adversarial patches affecting both modalities simultaneously.

C. Positions and content optimization of patches

Given the significant influence of patch position and content on attack performance, many studies have investigated their roles in adversarial patch design. For example, He et al. [27] distributed multiple adversarial patches across images, where position optimization was performed jointly for all patches, and structural loss was introduced to guide content optimization. Yang et al. [15] optimized the pixel values of adversarial patches through gradient ascent. Wu et al. [13] optimized patch positions through key facial regions and refined patch content using gradient-based algorithms with multi-objective loss functions. Li et al. [9] employed a generator–decoder architecture to produce constrained and dynamically transformed patch positions and textures, achieving end-to-end optimization through weighted fusion. Ma et al. [12] proposed a spatially mutable adversarial patch method that identifies key positions with the greatest impact on target identity using gradient search and iteratively optimizes patch textures with a texture gradient loss.

Despite their progress, these methods rely heavily on complex generators or internal model information and are constrained by the feature representation of specific detection

models and predefined key regions, making it difficult to achieve flexible adaptation in complex scenarios.

III. METHODOLOGY

A. Threat model

This paper conducts research on adversarial attacks against VI dense prediction tasks, with the core objective of generating adversarial patches with excellent attack effectiveness and relative stealthiness to interfere with the model outputs of three representative tasks, i.e., crowd counting, semantic segmentation, and image fusion. A black-box attack assumption is adopted in this research, the attacker does not need to acquire complete information such as the internal architecture and parameter configuration of the target model, and can implement effective attacks merely through output feedback.

Based on the above threat model, the paper proposes a global optimization framework that jointly searches for adversarial patches optimal position and color in a unified parameter space, guided by a fitness function and optimized via a global search mechanism. Its pipeline: encode patches into parameter vectors (position and color), generate initial candidate populations, iteratively update via global search (evaluate candidates using the fitness function, retain higher-fitness ones), and decode the best vector for the final patch upon convergence or max iterations. For clarity, the overall framework is illustrated in Fig 3 and the patch generation procedure is detailed in Algorithm 1.

Algorithm 1 Generate Adversarial Patch

Input: Clean visible image X_{vis} , clean infrared image X_{inf} , the fitness function $J(\cdot)$, the max number of iterations T
Output: Visible adversarial example X_{vis}^{adv} and infrared adversarial example X_{inf}^{adv} ;

- 1: Initialize Population $S(0)$
- 2: **for** $k = 0$ to $T-1$ **do**
- 3: Sort $S(k)$ in descending order according to $J(S(k))$
- 4: **if** $S_0(k)$ makes the attack successful **then**
- 5: stop = k ; break;
- 6: **end if**
- 7: Generate $S(k+1)$ based on crossover and mutation.
- 8: Limit boundaries of $S(k+1)$
- 9: **for** $i = 1$ to Q **do**
- 10: Evaluate $S_i(k)$ and $S_i(k+1)$
- 11: $S_i(k+1) \leftarrow$ the better one in $S_i(k)$ and $S_i(k+1)$
- 12: **end for**
- 13: **end for**
- 14: Sort $S(stop)$ in descending order according to $J(S(k+1))$
- 15: Choose $S_0(stop)$ as the final individual from $S(stop)$
- 16: Generate unified patch M with $S_0(stop)$ by integrating position (x, y) and color (R, G, B)
- 17: Obtain adversarial examples with M
- 18: **return** $X_{vis}^{adv}, X_{inf}^{adv}$

B. Problem formulation

In visual–infrared dense prediction tasks, a joint cross-modal adversarial attack takes a pair of clean visible and infrared images as input and generates perturbed counterparts by embedding an adversarial patch. The objective of the adversarial patch is to perturb the input in a way that interferes with the model output.

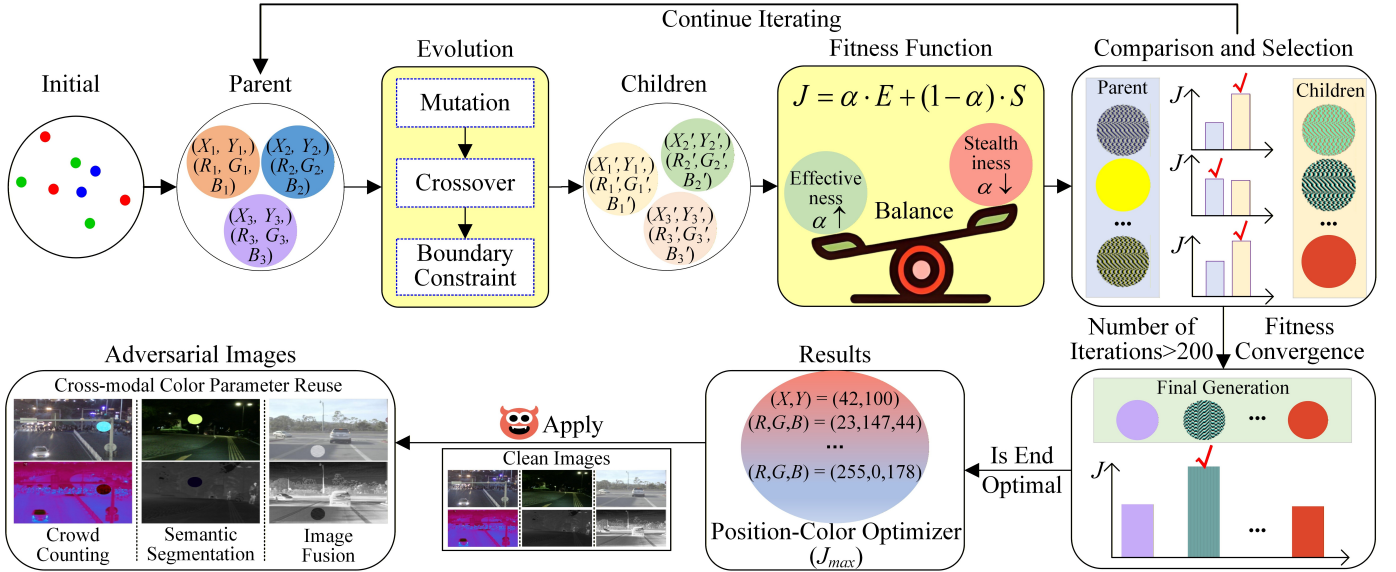


Fig. 3. Framework of cross-modal adversarial patches with position-color joint optimization. The initial population consists of a series of randomly generated circular samples. Then, through mutation, crossover, and boundary handling, a child population with diverse positions and colors is generated. A fitness function is then applied for cross-modal evaluation to compare the parent and child populations and repeat the iterative loop, ultimately obtaining the optimal patch deployed for dense prediction tasks.

Let X_{vis} and X_{inf} denote the original visible and infrared images of size $h \times w$. The adversarial images X_{vis}^{adv} and X_{inf}^{adv} are defined as

$$X_{vis}^{adv} = X_{vis} \odot (1 - M) + X'_{vis} \odot M, \quad (1)$$

$$X_{inf}^{adv} = X_{inf} \odot (1 - M) + X'_{inf} \odot M, \quad (2)$$

where $M \in \{0, 1\}^{h \times w}$ is a binary mask indicating the patch region. A value of $M_{ij}=1$ means that pixel (i, j) belongs to the patch, while $M_{ij}=0$ preserves the original image. The matrices X'_{vis} and X'_{inf} specify the pixel values of the patch in the visible and infrared modalities, respectively, and \odot denotes the Hadamard product.

C. Global Optimization Framework

In cross-modal patch optimization, the underlying search space exhibits highly non-convex and partially discontinuous characteristics. The spatial parameters (x, y, r) determine a binary mask M , which introduces discrete structural changes in the input space, while the color parameters define continuous perturbations within the selected region. This mixed discrete-continuous parameterization leads to a rugged fitness landscape with multiple local optima.

Furthermore, visual and infrared modalities possess heterogeneous spectral responses. A perturbation that induces strong activation changes in the visible branch may produce weak or inconsistent responses in the infrared branch. Such modality-dependent sensitivity further increases the irregularity of the optimization landscape. In dense prediction models, outputs are spatially aggregated across feature maps. Small changes in patch placement may therefore activate different local receptive fields, causing abrupt variations in the fitness landscape. As a result, the optimization problem becomes highly non-linear and sensitive to spatial placement.

Under the adopted black-box threat model, internal gradients and model parameters are unavailable. Even if numerical gradient approximation is applied, the discontinuity introduced by binary masks and modality-specific feature extraction may result in unstable or misleading update directions. Therefore, local gradient-based optimization methods are not well suited for exploring the combined spatial-spectral parameter space.

To address these challenges, we adopt a population-based global optimization strategy that can effectively explore disjoint feasible regions and escape local optima. Population-based methods maintain multiple candidate solutions simultaneously and update them through stochastic variation, enabling broader exploration of the search space.

Specifically, Differential Evolution (DE) is employed as the optimization backbone due to its strong global search capability, robustness to irregular objective landscapes, and suitability for mixed-parameter optimization. Within this framework, each individual encodes a complete set of patch parameters, including spatial position and color values. The population is iteratively refined according to the fitness function described in Section III-D, and the candidate with the highest fitness is selected as the final adversarial patch.

DE refines a population of candidate solutions through mutation, crossover, and selection. Compared with traditional evolutionary algorithms such as genetic algorithms or particle swarm optimization, DE provides faster convergence and stronger global exploration ability in high-dimensional parameter spaces. These properties make DE particularly suitable for optimizing adversarial patches in VI dense prediction tasks.

D. Fitness function

The optimization process is guided by a fitness function that evaluates the progress of cross-modal adversarial attacks. By measuring both the attack strength of the patch and its

stealthiness, the fitness function provides a clear direction for the iterative evolution of patch parameters, defined as

$$J = \alpha \cdot E(X^{adv}) + (1 - \alpha) \cdot S(X^{adv}), \quad (3)$$

where $\alpha \in [0, 1]$ controls the trade-off between attack effectiveness and stealthiness. A larger value of α places more weight on the effectiveness term $E(\cdot)$ and encourages the optimization to produce stronger attacks, while a smaller value places more emphasis on the stealthiness term $S(\cdot)$ and encourages less noticeable patches. The choice of α may be set through validation or adjusted according to specific attack–defense requirements. E denotes attack effectiveness, which has different formulations in various dense prediction tasks.

In the crowd counting task, E refers to the people count error (as shown in Eq. 4):

$$E_{count} = |\text{count}(X^{adv}) - \text{count}(X)|, \quad (4)$$

where X denotes the original image, X^{adv} denotes the adversarial image, $\text{count}(\cdot)$ denotes the function for calculating the number of people.

In the semantic segmentation task, it refers to the mIoU (as shown in Eq. 5):

$$E_{seg} = 100 - (mIoU(X^{adv}) \times 100), \quad (5)$$

where $mIoU(\cdot)$ denotes the function for calculating the mIoU value.

In the image fusion task, it uses gradient loss (\mathcal{L}_{grad}), intensity loss (\mathcal{L}_{inten}), and SSIM, as shown in Eq. 6:

$$\begin{aligned} E_{fus} &= \mathcal{L}_{inten}(X_{vis}, X_{inf}, X^{adv}) \times 20 \\ &+ \mathcal{L}_{grad}(X_{vis}, X_{inf}, X^{adv}) \times 20 \\ &+ (1 - SSIM(X_{vis}, X_{inf}, X^{adv})) \times 10, \end{aligned} \quad (6)$$

where X_{vis} and X_{inf} denote the original visible image and the infrared image, respectively.

S denotes stealthiness, employing SSIM and PSNR (Eq. 7) [28] in the crowd counting and semantic segmentation tasks.

$$\begin{aligned} S_{count}/S_{seg} &= (PSNR_{vis} + PSNR_{inf}) \times 1 \\ &+ (SSIM_{vis} + SSIM_{inf}) \times 20, \end{aligned} \quad (7)$$

where $PSNR_{vis}$ represents the PSNR value between the original image and the adversarial image in the visible modality, $SSIM_{vis}$ represents the SSIM value between the original image and the adversarial image in the visible modality, $PSNR_{inf}$ represents the PSNR value between the original image and the adversarial image in the infrared modality, and $SSIM_{inf}$ represents the SSIM value between the original image and the adversarial image in the infrared modality.

For crowd counting and semantic segmentation, attack effectiveness is evaluated using task-specific metrics (e.g., GAME, RMSE, mIoU), while stealthiness is measured with SSIM and PSNR, as these two aspects are negatively correlated. However, for the image fusion task, SSIM and PSNR already serve as the indicators of task performance, since fusion effectiveness inherently depends on the similarity between the fused image and the original inputs. Therefore, using SSIM or PSNR again to quantify stealthiness would create a coupling

between attack effectiveness and stealthiness, and thus the stealthiness metric is not considered for the fusion task.

E. Representation of patch position

The position of the adversarial patch is parameterized by a unified center coordinate (x, y) and a radius r , which determines the patch size. To ensure that the patch remains within image boundaries, the feasible region of the patch center is constrained by

$$x \in [r, w - r], \quad y \in [r, h - r], \quad (8)$$

where w and h denote the width and height of the image, respectively.

F. Representation of patch color

In addition to position, each adversarial patch is assigned a list of color values, where each color is represented by an $[R, G, B]$ triplet. After localizing all pixels within the circular patch region, the colors in the list are assigned sequentially to each pixel using a modulo operation. This cyclic assignment produces a multi-color pattern without increasing the dimensionality of the parameter space.

Visible and infrared images differ substantially in appearance and dynamic range, so directly applying visible colors to infrared images often produces unrealistic artifacts. To address this problem, we adopt a cross-modal color parameter reuse strategy. In the visible modality, the color mask is multiplied with the three-channel image to form a high-brightness region that strongly disrupts texture and color cues. In the infrared modality, the same color parameters are first converted to grayscale and then compressed in intensity, allowing the patch to blend naturally into the grayscale appearance of infrared images and avoiding abrupt visual patterns. This strategy improves stealthiness while maintaining strong perturbation capability across modalities.

G. Joint optimization

The optimization of patch position and color is performed jointly within a unified parameter vector. For each individual in the DE population, the vector contains both spatial parameters (x, y, r) and color parameters ($[R, G, B]$ values). The initial parent population is constructed from randomly generated patches. During optimization, for each V_m in the k -th population, three distinct individuals V_{m1} , V_{m2} , and V_{m3} are randomly selected to generate a mutation vector

$$V_{mut} = V_{m1} + f \cdot (V_{m2} - V_{m3}), \quad (9)$$

where f is the scaling factor controlling the influence of the differential pair. The mutation vector is combined with V_m through binomial crossover to form a trial vector

$$V_{trial}(j) = \begin{cases} V_{mut}(j) & \text{if } \text{rand}(0, 1) \leq CR \text{ or } j = J_{rand} \\ V_m(j) & \text{otherwise} \end{cases} \quad (10)$$

where $CR \in [0, 1]$ is the crossover probability, j denotes a parameter dimension, and $J_{rand} \in \{1, 2, \dots, D\}$ is a randomly selected index ensuring at least one mutated dimension.



Fig. 4. Variation trajectory of patch positions across iterations. Yellow markers denote the patch center coordinates of all individuals in each generation, while red markers indicate the center coordinate of the individual with the highest fitness in that generation. As iterations progress, the population gradually converges toward crowd-dense regions and ultimately stabilizes at the optimal patch location.

This process allows the search space to be explored effectively while preserving useful characteristics of the current solution. The fitness function defined in Section III-D is then computed for both the V_{trial} and the V_m , and the one with higher fitness is retained. This iterative process continues until the population converges or a fixed number of iterations (e.g., 200) is reached. As shown in Fig. 4, the individuals gradually converge toward the most effective patch location, and the color parameters are updated according to the balance between attack effectiveness and stealthiness defined by the weighting parameter α . The final output of the algorithm is the adversarial patch with the highest fitness value across the visible and infrared modalities.

H. Optimization Coupling Analysis

The patch generation process described previously can be interpreted as solving a joint optimization problem with respect to both spatial and color parameters. Specifically, guided by the fitness function defined in Eq. (3), the optimization objective can be written as

$$\max_{x,y,r,c} J(X_{vis}^{adv}, X_{inf}^{adv}), \quad (11)$$

where (x, y, r) denote the spatial parameters determining the patch mask M , and c denotes the set of color parameters controlling the patch content in both modalities.

As defined in Eqs. (1)–(2), the adversarial images are constructed by embedding the patch mask $M(x, y, r)$ and the corresponding color-dependent patch contents into the original visible and infrared images. Therefore, the fitness value J is an implicit function of both the spatial support region and the color-induced perturbation magnitude.

In dense prediction tasks, model outputs are computed from spatially distributed feature responses. The perturbation introduced by an adversarial patch affects a set of pixels determined by the mask $M(x, y, r)$, and its influence on the fitness function can be approximated as

$$\Delta J \approx \sum_{(i,j) \in M(x,y,r)} \frac{\partial J}{\partial X_{i,j}} \cdot \delta X_{i,j}, \quad (12)$$

where $\delta X_{i,j}$ is determined by the color parameters c .

This expression reveals the intrinsic coupling between spatial and color parameters. The spatial parameters (x, y, r) determine which pixel locations contribute to the perturbation, while the color parameters determine the direction and magnitude of perturbation at those locations. Consequently, the effect of a given color configuration depends on the selected spatial region, and vice versa.

Optimizing position while fixing color restricts the perturbation direction in feature space, whereas optimizing color under a fixed position limits the exploitable spatial sensitivity of the model. Independent optimization therefore constrains the reachable perturbation subspace and may lead to suboptimal local solutions. This observation implies that the optimization problem is inherently inseparable in spatial and spectral dimensions.

This coupling effect becomes more pronounced in VI settings. The visible modality operates in a three-channel RGB space, whereas the infrared modality primarily relies on intensity information. Furthermore, multimodal fusion modules aggregate spatial and spectral cues jointly. As a result, the sensitivity of J to perturbations depends simultaneously on spatial placement and cross-spectral consistency. Joint optimization enables coordinated exploration in the combined spatial–spectral parameter space, leading to stronger cross-modal perturbations and improved attack effectiveness in dense prediction tasks.

IV. EXPERIMENTS

A. Experimental settings

1) *Implementation details*: During the iterative optimization process, the fitness function was set to consider only attack effectiveness ($\alpha = 1$) for the main experiments. This unified setting allows fair comparison across models and tasks, as the primary goal of these experiments is to evaluate the attack effectiveness of the proposed method under a consistent configuration. To demonstrate the flexibility of the framework, additional experiments in Section IV-B3 analyze different values of α and show how the weighting factor can adjust the balance between attack effectiveness and stealthiness.

For crowd counting, semantic segmentation, and image fusion, the patch radius was set to 40, 40, and 30 pixels, with the number of colors in the patch color list set to 10, 10, and 2, respectively. The maximum number of iterations is uniformly set to 200 for all tasks.

2) *Datasets*: We conduct experiments on three publicly available datasets: the RGBT-CC dataset [29], the MF dataset [30], and the RoadScene dataset [31]. These datasets contain paired visible and infrared images and correspond to three representative tasks: crowd counting, semantic segmentation, and image fusion, respectively. This selection ensures both the diversity and representativeness of the experimental data. Following the protocol in reference [32], we randomly sample 100 images from the test set of each dataset using

TABLE I

COMPARISON OF EXPERIMENTAL RESULTS WITH EXISTING METHODS. SINGLE-MODAL ADVERSARIAL PATCH METHODS ADAPTED TO THE CROSS-MODAL BL+IADM CROWD COUNTING MODEL. “PSNR_RGB” AND “PSNR_T” DENOTE THE PSNR VALUES FOR VISIBLE IMAGES AND INFRARED IMAGES, RESPECTIVELY. “SSIM_RGB” AND “SSIM_T” DENOTE THE SSIM VALUES FOR VISIBLE IMAGES AND INFRARED IMAGES, RESPECTIVELY. **BOLD** INDICATES THE BEST RESULTS.

	Effectiveness					Stealthiness			
	GAME(0)↑	GAME(1)↑	GAME(2)↑	GAME(3)↑	RMSE↑	PSNR_RGB↑	SSIM_RGB↑	PSNR_T↑	SSIM_T↑
Clean	13.7001	18.3601	22.1256	28.6380	24.4166	-	-	-	-
PAP	14.9798	20.9912	26.6463	33.4813	25.1726	23.5981	0.9768	23.7474	0.9747
APAM	14.6624	19.1693	23.1393	30.0921	25.9723	28.0505	0.9822	26.7175	0.9738
AP-PCO(Ours)	40.5543	51.2453	56.7172	63.6817	45.1786	25.6450	0.9832	28.2151	0.9850

a fixed random seed with the selected samples covering diverse scenes to ensure reproducibility and cross-experiment comparability.

3) *Target models*: We select several representative models from each task as the target models. For the crowd counting task, BL+IADM [29], CAGNet [33], and CFAFNet [34] were employed. For the semantic segmentation task, Openres [35], FEANet [36], and SGFNet [37] were used. For the image fusion task, Res2Fusion [38], UNFusion [39], and MaeFuse [40] served as the evaluation models. All models are initialized and constructed using official pre-trained weights to ensure reliable and consistent experimental benchmarks.

4) *Evaluation metrics*: We evaluate attack methods from two perspectives: attack effectiveness and stealthiness. Details are as follows:

Attack Effectiveness for Crowd Counting: Grid Average Mean Absolute Error (GAME(k))(Eq. 13) and Root Mean Square Error (RMSE)(Eq. 14) [41] are adopted as evaluation metrics:

$$\text{GAME}(k) = \frac{1}{n} \sum_{i=1}^n \sum_{j=1}^{4^k} |y_i^j - \hat{y}_i^j|, \quad (13)$$

$$\text{RMSE} = \sqrt{\frac{1}{n} \sum_{i=1}^n (y_i - \hat{y}_i)^2}, \quad (14)$$

where n is the number of samples; k determines the number of grids: 4^k indicates that the sample is divided into uniform 4^k sub-grids. y_i^j and \hat{y}_i^j denote the estimated counting and corresponding GT counts in region j of image i , respectively; y_i and \hat{y}_i denote the estimated counting and corresponding GT counts of image i , respectively. **Higher values** of GAME(k) and RMSE indicate stronger degradation of the model’s prediction accuracy, **reflecting higher attack effectiveness**.

Attack Effectiveness for Semantic Segmentation: Mean Intersection over Union (mIoU) (Eq. 15) and Recall (Eq. 16) are adopted as evaluation metrics:

$$\text{mIoU} = \frac{1}{n-1} \sum_{i=0}^n (P_{ii} / (\sum_{j=0}^n (p_{ij} + P_{ji}) - P_{ii})), \quad (15)$$

$$\text{Recall} = \frac{1}{n+1} \sum_{i=0}^n (P_{ii} / \sum_{j=0}^n p_{ji}), \quad (16)$$

where n denotes the number of manually annotated object categories, and P_{ij} is the number of pixels belonging to category i that are predicted as category j . The combination of these two metrics provides a comprehensive assessment of the attack’s

impact on model performance. Under adversarial conditions, **lower values** of mIoU and Recall **indicate stronger attack effectiveness**.

Attack Effectiveness for Image Fusion: Qabf [42], SSIM, PSNR, Visual Information Fidelity (VIFF) [43], and Correlation Coefficient (CC) [44] are adopted as evaluation metrics. **Lower values** of Qabf, SSIM, PSNR, VIFF, and CC indicate stronger degradation of fusion quality, **reflecting higher attack effectiveness**.

Attack Stealthiness: To assess the stealthiness of the adversarial patches generated by the proposed method, two widely used image quality assessment metrics, SSIM and PSNR, are adopted. Higher PSNR values correspond to lower pixel-level distortion and greater visual similarity to the original image. SSIM ranges from 0 to 1, with values closer to 1 indicating stronger structural consistency between the adversarial and original images.

B. Attacks in the Digital World

1) *Compare with other adversarial patch methods*: Existing adversarial patch attack methods for dense prediction tasks mainly focus on the visible modality, whose attack objectives, input forms, and optimization strategies are all based on the single-modality assumption. Consequently, they are difficult to be directly migrated to the VI dense prediction tasks with visible and infrared inputs, and extensive structural adjustments to the patch embedding method, optimization objective, and inter-modal feature alignment strategy are required when applied to cross-modal tasks. To verify their applicability, this paper selects two representative methods PAP [10] and APAM [24], extends them to the cross-modal crowd counting BL+IADM model for comparative experiments without changing their core optimization mechanisms. As shown in Table I, the experimental results indicate that single-modality patch methods fail to achieve stable and effective attack effects in VI dense prediction tasks.

2) *Attack performance against different models*: We evaluate the attack performance of the proposed method across multiple mainstream model architectures to assess its generalization and robustness. As shown in the experimental results in Tables II–IV, which correspond to the crowd counting, semantic segmentation, and image fusion tasks, and in the visualizations in Fig. 5, the optimized patches generated by our method achieve strong attack performance across all evaluated models. Although SSIM and PSNR values show a slight decrease compared with images containing randomly placed

TABLE II
ATTACK EFFECTIVENESS AND STEALTHINESS OF OUR METHOD ON DIFFERENT MODELS FOR THE CROWD COUNTING TASK. “CLEAN” DENOTES THE ORIGINAL IMAGE, “RANDOM” DENOTES IMAGES WITH PATCHES ADDED USING RANDOMLY SAMPLED POSITIONS AND COLORS.

Model	Settings	Effectiveness					Stealthiness			
		GAME(0)↑	GAME(1)↑	GAME(2)↑	GAME(3)↑	RMSE↑	PSNR_RGB↑	SSIM_RGB↑	PSNR_T↑	SSIM_T↑
BL+IADM	Clean	13.70	18.36	22.13	28.64	24.42	-	-	-	-
	Random	14.20	18.80	22.80	29.32	24.36	27.01	0.99	31.31	0.99
	AP-PCO (Ours)	40.55	51.25	56.72	63.68	45.18	25.65	0.98	28.22	0.99
CAGNet	Clean	11.15	14.43	18.19	23.37	17.66	-	-	-	-
	Random	11.41	14.66	18.41	23.56	18.12	27.04	0.99	31.28	0.99
	AP-PCO (Ours)	21.05	25.78	29.69	34.31	29.20	24.77	0.98	26.84	0.98
CFAFNet	Clean	11.15	14.91	19.01	26.27	17.15	-	-	-	-
	Random	11.11	15.78	20.22	27.34	16.40	26.73	0.95	31.11	0.96
	AP-PCO (Ours)	59.19	69.86	75.38	83.18	63.17	24.78	0.98	26.77	0.98

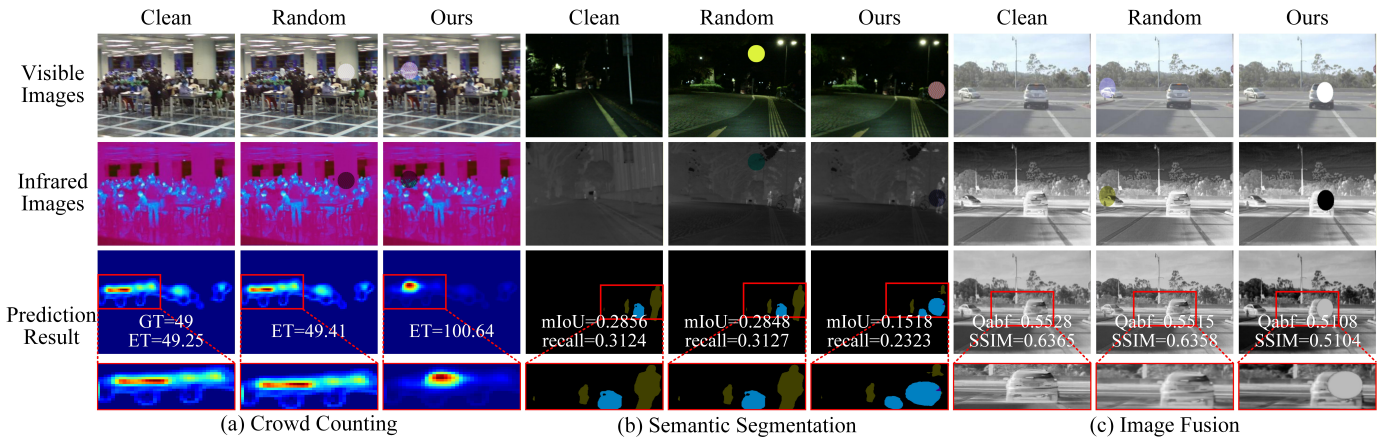


Fig. 5. Visualizations of patch attacks for the crowd counting, semantic segmentation, and image fusion tasks. As can be seen, the proposed method shows strong attack performance across three VI dense prediction tasks.

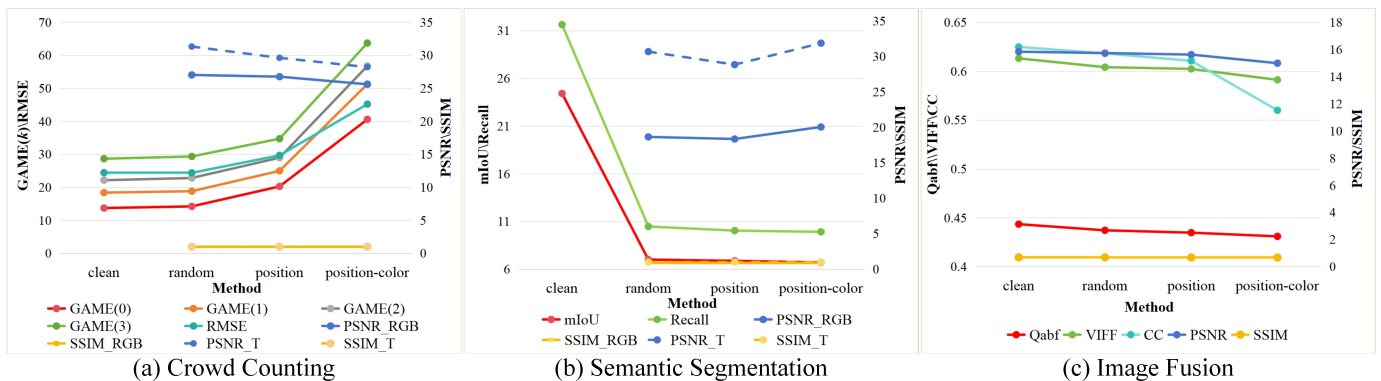


Fig. 6. Comparison of ablation experiment results for the crowd counting task (BL+IADM model), the semantic segmentation task (Openpress) and the image fusion task (UNFusion). In this figure, “clean” denotes the original image; “random” denotes images with randomly added patches in both positions and color; “position” denotes images with patches optimized only for positions while color remains random; and “position-color” denotes images with patches optimized for both positions and color.

patches, this result is expected. Combined with the stronger attack effectiveness and visualization results, it indicates that the proposed method achieves a more reasonable trade-off between attack intensity and relative stealth, thereby verifying the effectiveness of the stealthiness enhancement strategy.

3) *Ablation studies:* To verify the effectiveness of each module in the proposed method, a series of ablation experiments is designed and conducted.

Result Stability Analysis: Although evaluation is conducted on a subset of 100 test images, the results exhibit stable

and consistent degradation across samples. As shown in Table V, the standard deviation remains nearly unchanged after the attack. The result indicates consistent performance degradation across samples, meaning that the model’s prediction errors for all test samples increased by approximately the same margin at the original dispersion level, and there is no significant variation in attack effectiveness across samples. The relatively large variance mainly stems from the inherent density variation between sparse and highly congested scenes, which is common in crowd counting benchmarks.

TABLE III

ATTACK EFFECTIVENESS AND STEALTHINESS OF THE PROPOSED METHOD ON DIFFERENT MODELS FOR THE SEMANTIC SEGMENTATION TASK.

Model	Settings	Effectiveness		Stealthiness			
		mIoU↓	Recall↓	PSNR_RGB↑	SSIM_RGB↑	PSNR_T↑	SSIM_T↑
Open res	Clean	24.41	31.63	-	-	-	-
	Random	6.99	10.64	18.65	0.86	30.69	0.98
	AP-PCO (Ours)	6.69	9.90	20.05	0.86	31.88	0.98
FEA Net	Clean	52.52	70.68	-	-	-	-
	Random	50.32	68.06	21.50	0.86	36.12	0.99
	AP-PCO (Ours)	1.58	10.91	20.45	0.86	32.36	0.98
SGF Net	Clean	53.40	66.47	-	-	-	-
	Random	52.58	66.06	21.34	0.86	35.86	0.99
	AP-PCO (Ours)	39.62	56.78	20.72	0.85	33.35	0.98

TABLE IV

ATTACK EFFECTIVENESS AND STEALTHINESS OF THE PROPOSED METHOD ON DIFFERENT MODELS FOR THE IMAGE FUSION TASK.

Model	Setting	Qabf↓	PSNR↓	SSIM↓	VIFF↓	CC↓
UNFusion	Clean	0.52	13.89	0.65	0.74	0.61
	Random	0.51	13.88	0.64	0.72	0.60
	AP-PCO (Ours)	0.50	13.50	0.64	0.72	0.56
Res2Fusion	Clean	0.44	15.84	0.68	0.61	0.62
	Random	0.44	15.74	0.67	0.60	0.62
	AP-PCO (Ours)	0.43	15.00	0.67	0.59	0.56
MaeFuse	Clean	0.46	15.81	0.68	0.56	0.65
	Random	0.46	15.81	0.68	0.55	0.65
	AP-PCO (Ours)	0.46	15.66	0.67	0.55	0.64

TABLE V

STABILITY ANALYSIS OF ADVERSARIAL ATTACK PERFORMANCE FOR BL+IADM CROWD COUNTING MODEL (MEAN ± STD).

	GAME(0)↑	GAME(1)↑	GAME(2)↑	GAME(3)↑	RMSE↑
clean	13.70±19.99	18.36±19.90	22.13±20.35	28.64±22.21	24.42±20.06
AP-PCO(Ours)	40.55±19.73	51.25±19.83	56.72±20.29	63.68±21.13	45.18±20.00

TABLE VI

EFFECT OF THE CROSS-MODAL COLOR PARAMETER REUSE STRATEGY ON THE SEMANTIC SEGMENTATION TASK.

	Effectiveness		Stealthiness			
	mIoU↓	Recall↓	PSNR_RGB↑	SSIM_RGB↑	PSNR_T↑	SSIM_T↑
Not used	36.06	42.86	20.4394	0.8543	26.2563	0.9802
Used	39.62	56.78	20.7228	0.8544	33.3521	0.9835

Effect of patch position-color optimization: We conduct comparative experiments under two settings: one that applies the global search mechanism to position optimization only, and another that performs joint position and color optimization. As shown in Fig. 6, the proposed joint optimization strategy produces adversarial patches with stronger attack effectiveness and also improves relative stealthiness in dense prediction tasks.

Effect of cross-modal color parameter reuse: We conduct comparative experiments with and without the color reuse mechanism. As shown in Table VI, the reuse strategy significantly improves stealthiness and avoids the noticeable artifacts that appear when visible-domain colors are directly applied to infrared images. The improvement is particularly evident in the infrared modality, where signal integrity is better preserved. Although attack effectiveness decreases slightly, this trade-off is expected because the reuse mechanism prioritizes stealthiness by suppressing excessive perturbations. Overall, the results demonstrate that the proposed strategy achieves a more balanced trade-off between attack strength

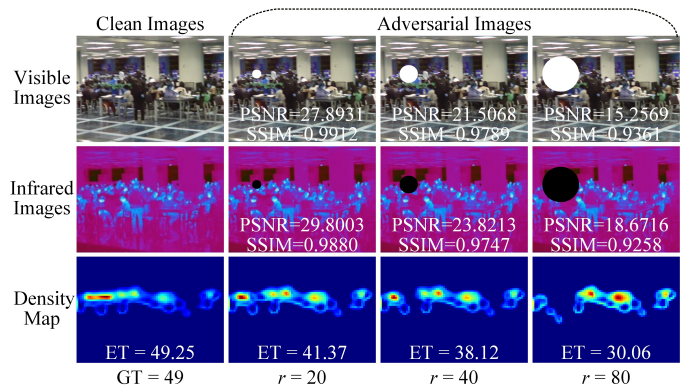


Fig. 7. Visualization of patch radius parameters attack performance. As the radius of the adversarial patch increases, its occlusion ratio in the image gradually rises, resulting in a significant degradation of stealthiness in cross-modal scenarios.

and stealthiness.

Effect of cross-modal attacks: We conduct ablation experiments using three strategies: attacking only the infrared modality, attacking only the visible modality, and attacking both modalities simultaneously. As shown in Table VII, the cross-modal attack achieves stronger attack performance than either single-modality one, demonstrating the advantage of simultaneously perturbing both visible and infrared modalities.

Effect of fitness function: We conduct comparative experiments on crowd counting and semantic segmentation tasks using two settings: one that considers only attack effectiveness ($\alpha = 1$) and another that jointly considers attack effectiveness and stealthiness ($\alpha = 0.5, \alpha = 0.1$). Table VIII and IX show the effectiveness of α in the fitness function for adjusting the trade-off between attack strength and stealthiness, and the framework can adapt to different task requirements.

4) Hyperparameter Settings: We conduct the following experiments to investigate the impact of the patch hyperparameters (iteration epochs, patch sizes, and the number of colors) on attack performance.

Patch Sizes: We control the patch size by adjusting the radius r of the circular patch to 20, 40, and 80. As shown in Table X, both GAME and RMSE increase as the patch size grows, indicating enhanced attack effectiveness. However, the occlusion rate also increases, reducing stealthiness. As shown in Fig. 7, larger patches cover more irrelevant regions of the image and are more perceptible. Considering the trade-off between attack effectiveness and stealthiness, we choose a radius of $r = 40$. For the semantic segmentation and image fusion tasks, the patch radius is set to 40 and 30 pixels based on the respective image sizes.

Color Numbers: We conduct experiments using 1, 2, 5, and 10 colors. Based on the results in Tables XI, XII, and XIII, we select 10 colors for the crowd counting and semantic segmentation tasks, and 2 colors for the image fusion task.

Iteration Epochs: The epochs represent the maximum number of evolution iterations for a single image. Although increasing epochs generally improves attack performance via broader search, it drastically raises computational cost. Therefore, the number of epochs is first set to 200, and an early stop-

TABLE VII

EFFECT OF DIFFERENT ATTACK MODALITIES OF THREE DENSE PREDICTION TASKS. “VISIBLE” AND “INFRARED” DENOTE ATTACKS APPLIED TO THE VISIBLE OR INFRARED MODALITY ONLY, WHILE “VI” DENOTES ATTACKS APPLIED TO BOTH MODALITIES SIMULTANEOUSLY.

Modal	Crowd Counting					Semantic Segmentation		Image Fusion				
	GAME(0)↑	GAME(1)↑	GAME(2)↑	GAME(3)↑	RMSE↑	mIoU↓	Recall↓	Qabf↓	PSNR↓	SSIM↓	VIFF↓	CC↓
Visible	21.3622	25.8889	30.4938	36.2902	30.7622	6.97	9.96	0.4347	15.0853	0.6672	0.5956	0.5668
Infrared	36.9179	47.8553	54.7607	62.1525	43.8502	7.56	10.75	0.4347	15.1014	0.6710	0.5963	0.5695
VI	40.5543	51.2453	56.7172	63.6817	45.1786	6.69	9.90	0.4309	14.9952	0.6659	0.5912	0.5600

TABLE VIII

EFFECT OF DIFFERENT FITNESS FUNCTION WEIGHTS ON THE CROWD COUNTING TASK.

α	Effectiveness					Stealthiness			
	GAME(0)↑	GAME(1)↑	GAME(2)↑	GAME(3)↑	RMSE↑	PSNR_RGB↑	SSIM_RGB↑	PSNR_T↑	SSIM_T↑
1	39.5844	53.0996	61.2997	68.8205	44.4267	25.2850	0.9792	28.1450	0.9792
0.5	39.2131	51.5339	61.2194	69.1666	46.6531	26.4535	0.9800	28.8502	0.9799
0.1	30.8848	43.2991	50.7023	58.2660	38.2710	32.8543	0.9855	33.6389	0.9837

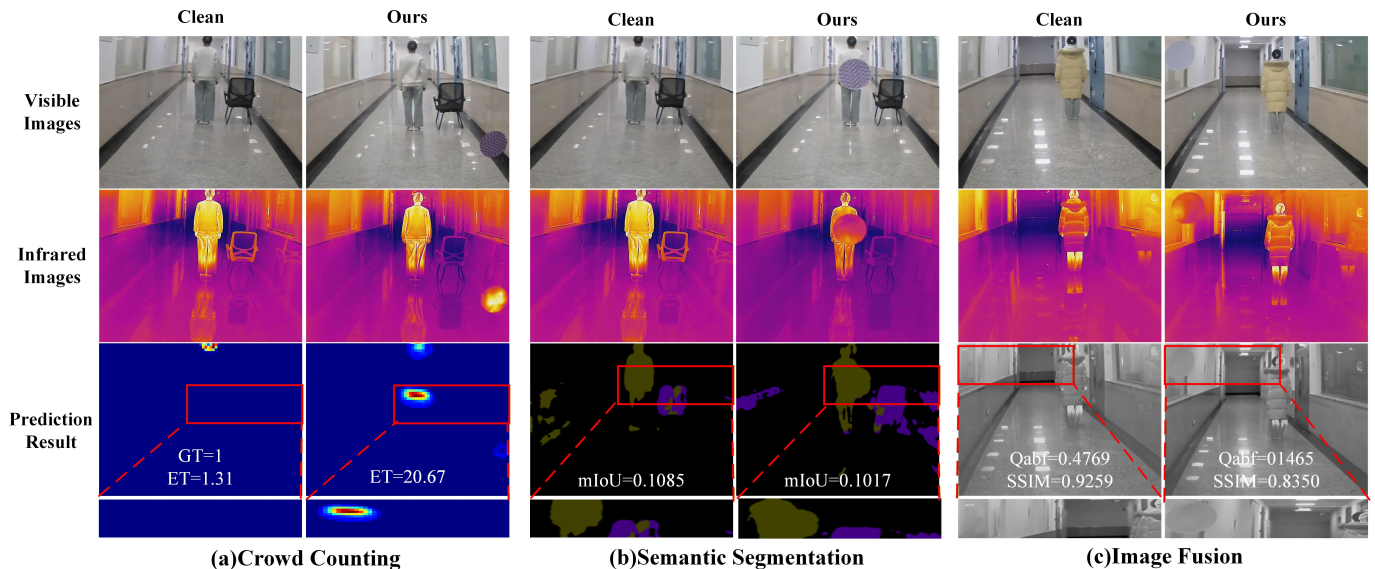


Fig. 8. Visualization results of adversarial patches against physical attacks in crowd counting, semantic segmentation, and image fusion tasks. As can be seen, the proposed method shows strong attack performance across three VI dense prediction tasks.

TABLE IX

EXPERIMENTAL RESULTS ON DIFFERENT FITNESS FUNCTION WEIGHTS FOR THE SEMANTIC SEGMENTATION TASK.

α	Effectiveness			Stealthiness		
	mIoU ↓	Recall ↓	PSNR_RGB ↑	SSIM_RGB ↑	PSNR_T ↑	SSIM_T ↑
1	6.69	9.90	20.0540	0.8612	31.8827	0.9834
0.5	6.88	10.36	24.7938	0.8734	59.0620	0.9996
0.1	6.88	10.36	24.7985	0.8736	59.2910	0.9996

ping mechanism is adopted to automatically stop optimization for a sample when its mean fitness value remains unchanged for 10 consecutive generations (the fitness function converges). Experimental results show that approximately 12%, 60%, and 21% of samples converged early on the crowd counting, semantic segmentation, and image fusion tasks, respectively. This indicates that some samples can achieve stable attack performance with fewer iterations, while setting the maximum number of iterations to 200 can provide sufficient search space for the remaining samples to enhance attack performance. Considering both attack performance and time efficiency, the

number of epochs is set to 200.

C. Attacks in the Physical World

To verify the effectiveness of the adversarial patches in the physical world, we select a laboratory corridor as a representative scenario to conduct real-world image capture and physical attack validation, as shown in Fig. 8. Experimental results demonstrate that the generated adversarial patches exhibit attack performance in the three tasks: crowd counting, semantic segmentation, and image fusion. If applied to practical scenarios, they will pose potential security risks to the relevant fields relying on VI dense prediction systems.

D. Defense Against Adversarial Patches

This paper verifies three typical defense methods: Joint Photographic Experts Group (JPEG) compression [45], median filter(MF) [46], and mean square error (MSE)-based anomaly detection [47]. The experimental results are shown in Table XIV, and none of the methods achieve the defense effect:

TABLE X
EXPERIMENTAL RESULTS ON THE PATCH RADIUS PARAMETER OF THE BL+IADM MODEL FOR THE CROWD COUNTING TASK.

	Effectiveness					Stealthiness			
	GAME(0)↑	GAME(1)↑	GAME(2)↑	GAME(3)↑	RMSE↑	PSNR_RGB↑	SSIM_RGB↑	PSNR_T↑	SSIM_T↑
Clean	13.7001	18.3601	22.1256	28.6380	24.4166	-	-	-	-
r=20	20.3511	25.2802	29.4354	35.0948	29.6377	29.7634	0.9922	31.1696	0.9901
r=40	25.8050	30.3045	33.6848	38.7906	34.7603	22.8577	0.9864	25.3934	0.9854
r=80	34.1544	39.5820	42.4527	47.1011	44.3972	17.4165	0.9518	20.2550	0.9475

TABLE XI
EXPERIMENTAL RESULTS ON THE PATCH COLOR NUMBER PARAMETER OF THE BL+IADM MODEL FOR THE CROWD COUNTING TASK.

	Effectiveness					Stealthiness			
	GAME(0)↑	GAME(1)↑	GAME(2)↑	GAME(3)↑	RMSE↑	PSNR_RGB↑	SSIM_RGB↑	PSNR_T↑	SSIM_T↑
Clean	13.7001	18.3601	22.1256	28.6380	24.4166	-	-	-	-
Color=1	25.8050	30.3045	33.6848	38.7906	34.7603	22.8577	0.9864	25.3934	0.9854
Color=2	25.2305	30.2875	33.9155	39.0918	33.5994	23.8335	0.9816	25.8799	0.9797
Color=5	28.8294	34.7558	39.1652	45.1211	36.9115	24.4387	0.9836	27.1367	0.9848
Color=10	39.5943	51.1300	56.8469	63.9860	44.1738	25.6450	0.9832	28.2151	0.9850

TABLE XII
EXPERIMENTAL RESULTS ON THE PATCH COLOR NUMBER PARAMETER OF THE OPENRESS MODEL FOR THE SEMANTIC SEGMENTATION TASK.

	Effectiveness		Stealthiness			
	mIoU ↓	Recall ↓	PSNR_RGB↑	SSIM_RGB↑	PSNR_T↑	SSIM_T↑
Clean	24.41	31.63	-	-	-	-
Color=1	6.65	9.96	19.1507	0.8645	29.8579	0.9833
Color=2	6.71	9.94	19.3025	0.8625	30.3935	0.9829
Color=5	6.69	9.92	19.7081	0.8614	30.8039	0.9835
Color=10	6.69	9.90	20.0540	0.8612	31.8827	0.9834

TABLE XIII
EXPERIMENTAL RESULTS ON THE PATCH COLOR NUMBER PARAMETER OF THE RES2FUSION MODEL FOR THE IMAGE FUSION TASK.

	Qabf ↓	PSNR ↓	SSIM ↓	VIFF ↓	CC ↓
Clean	0.4434	15.8424	0.6784	0.6132	0.6249
Color=1	0.4305	15.0364	0.6662	0.5912	0.5618
Color=2	0.4309	14.9952	0.6659	0.5912	0.5600
Color=5	0.4393	15.2879	0.6613	0.6005	0.5847
Color=10	0.4393	15.2915	0.6615	0.6002	0.5843

JPEG compression removes high-frequency image components and disrupts the fine textures and high-frequency perturbation features of adversarial patches. MF smooths local pixels and suppresses sharp noise patterns, slightly weakening the attack performance. The MSE-based anomaly detection method identifies attack samples by calculating the mean square error between the predicted density map and the real annotation, and can only detect 22% of the attack samples. In summary, the experiments demonstrate that the adversarial patches proposed in this paper have strong robustness and can

TABLE XIV
EXPERIMENTAL RESULTS OF DEFENSE METHODS ON THE CROWD COUNTING TASK.

	GAME(0)	GAME(1)	GAME(2)	GAME(3)	RMSE
clean	13.7001	18.3601	22.1256	28.6380	24.4166
JPEG	30.0835	40.1116	45.5558	52.6953	36.6276
MF	30.2246	41.7568	47.1867	54.3790	36.6903
AP-PCO(Ours)	40.5543	51.2453	56.7172	63.6817	45.1786

effectively resist a variety of classical defense strategies.

V. CONCLUSIONS

This work presents a cross-modal joint optimization framework that uses global search to optimize the positions and colors of adversarial patches for visible and infrared images. A cross-modal color reuse strategy adapts a shared set of color parameters to both modalities, enabling effective disruption of multimodal feature representations while maintaining low saliency. Experiments on crowd counting, semantic segmentation, and image fusion show that the generated patches consistently degrade performance across diverse network architectures and effectively evade representative existing defense methods. These results verify the effectiveness and generalizability of cross-modal adversarial patch attacks and their prominent robustness further reveals the security vulnerabilities inherent in existing multimodal perception systems. Overall, this study advances the understanding of multimodal AI security and provides a practical tool for evaluating the vulnerability of multimodal perception models. It should be noted that our method still has certain limitations: physical world interference factors, such as variations in camera viewing angles and illumination conditions, may degrade the attack effectiveness of cross-modal adversarial patches in real-world scenarios. A systematic investigation and validation of these physical influencing factors will serve as an important direction for future work.

REFERENCES

- [1] X. Qin, Y. Cui, S. Sun, R. Chen, W. Ren, A. Knoll, and X. Cao, "Disentangle to fuse: Towards content preservation and cross-modality consistency for multi-modality image fusion," *IEEE Transactions on Image Processing*, pp. 1–1, 2026.
- [2] P. Duan, S. Jin, X. Lu, L. Liang, X. Kang, and A. Plaza, "Domain-adaptive mamba for cross-scene hyperspectral image classification," *IEEE Transactions on Image Processing*, pp. 1–1, 2026.
- [3] X. Zhang and Y. Demiris, "Visible and infrared image fusion using deep learning," *IEEE Transactions on Pattern Analysis and Machine Intelligence*, vol. 45, no. 8, pp. 10 535–10 554, 2023.
- [4] Q. D. M. Phan, "Evaluating the robustness of deep learning models against adversarial attacks," Master's thesis, Oslo Metropolitan University, 2024.

- [5] B. Luo, D. Liu, X. Peng, H. Zuo, J. Zhang, M. Li, and Y. Wei, "Progressive transformer with multi-modality adaptation for rgb-t tracking," *IEEE Transactions on Instrumentation and Measurement*, 2025.
- [6] W. Kong, H. Li, and F. Zhao, "Multi-scale modality-similar learning guided weakly supervised rgb-t crowd counting," *IEEE Sensors Journal*, 2024.
- [7] Y. Chen, X. Li, C. Luan, W. Hou, H. Liu, Z. Zhu, L. Xue, J. Zhang, D. Liu, X. Wu *et al.*, "Cross-level interaction fusion network-based rgb-t semantic segmentation for distant targets," *Pattern Recognition*, vol. 161, p. 111218, 2025.
- [8] J. Chen, L. Yang, W. Yu, W. Gong, Z. Cai, and J. Ma, "Sdsfusion: A semantic-aware infrared and visible image fusion network for degraded scenes," *IEEE Transactions on Image Processing*, 2025.
- [9] X. Li and S. Ji, "Generative dynamic patch attack," *arXiv preprint arXiv:2111.04266*, 2021.
- [10] S. Liu, J. Wang, A. Liu, Y. Li, Y. Gao, X. Liu, and D. Tao, "Harnessing perceptual adversarial patches for crowd counting," in *Proceedings of the 2022 ACM SIGSAC conference on computer and communications security*, 2022, pp. 2055–2069.
- [11] J. Shack, K. Petrovic, and O. Saukh, "Breaking the illusion: Real-world challenges for adversarial patches in object detection," *arXiv preprint arXiv:2410.19863*, 2024.
- [12] H. Ma, K. Xu, X. Jiang, Z. Zhao, and T. Sun, "Transferable black-box attack against face recognition with spatial mutable adversarial patch," *IEEE Transactions on Information Forensics and Security*, vol. 18, pp. 5636–5650, 2023.
- [13] Z. Wu, Y. Cheng, S. Zhang, X. Ji, and W. Xu, "Uniid: Spoofing face authentication system by universal identity," in *Proceedings of Network and Distributed System Security Symposium (NDSS)*, 2024.
- [14] T. Chakraborty, U. R. KS, S. M. Naik, M. Panja, and B. Manvitha, "Ten years of generative adversarial nets (gans): a survey of the state-of-the-art," *Machine Learning: Science and Technology*, vol. 5, no. 1, p. 011001, 2024.
- [15] X. Yang, F. Wei, H. Zhang, and J. Zhu, "Design and interpretation of universal adversarial patches in face detection," in *European Conference on Computer Vision*. Springer, 2020, pp. 174–191.
- [16] A. Abomakhelb, K. A. Jalil, A. G. Buja, A. Alhammedi, and A. M. Alenezi, "A comprehensive review of adversarial attacks and defense strategies in deep neural networks," *Technologies*, vol. 13, no. 5, p. 202, 2025.
- [17] M. Guo, L. Yuan, Z. Yan, B. Chen, Y. Wang, and Q. Ye, "Regressor-segmenter mutual prompt learning for crowd counting," in *Proceedings of the IEEE/CVF Conference on Computer Vision and Pattern Recognition*, 2024, pp. 28 380–28 389.
- [18] S. Cheng, P. Li, K. Han, and H. Xu, "Feature-aware transferable adversarial attacks against image classification," *Applied Soft Computing*, vol. 161, p. 111729, 2024.
- [19] C. H. Wu, J. Y. Koh, R. Salakhutdinov, D. Fried, and A. Raghunathan, "Adversarial attacks on multimodal agents," *arXiv e-prints*, pp. arXiv:2406, 2024.
- [20] K. Barik, S. Misra, and L. Fernandez-Sanz, "Adversarial attack detection framework based on optimized weighted conditional stepwise adversarial network," *International Journal of Information Security*, vol. 23, no. 3, pp. 2353–2376, 2024.
- [21] H. Wei, H. Tang, X. Jia, Z. Wang, H. Yu, Z. Li, S. Satoh, L. Van Gool, and Z. Wang, "Physical adversarial attack meets computer vision: A decade survey," *IEEE Transactions on Pattern Analysis and Machine Intelligence*, vol. 46, no. 12, pp. 9797–9817, 2024.
- [22] H. Fang, A. Liu, H. Yuan, J. Zheng, D. Zeng, Y. Liu, J. Deng, S. Escalera, X. Liu, J. Wan *et al.*, "Unified physical-digital face attack detection," *arXiv preprint arXiv:2401.17699*, 2024.
- [23] T. B. Brown, D. Mané, A. Roy, M. Abadi, and J. Gilmer, "Adversarial patch," *arXiv preprint arXiv:1712.09665*, 2017.
- [24] Q. Wu, Z. Zou, P. Zhou, X. Ye, B. Wang, and A. Li, "Towards adversarial patch analysis and certified defense against crowd counting," in *Proceedings of the 29th ACM International Conference on Multimedia*, 2021, pp. 2195–2204.
- [25] H. Sun, S. Wu, and L. Ma, "Adversarial attacks on gan-based image fusion," *Information Fusion*, vol. 108, p. 102389, 2024.
- [26] Z. Liu, J. Liu, B. Zhang, L. Ma, X. Fan, and R. Liu, "Paif: Perception-aware infrared-visible image fusion for attack-tolerant semantic segmentation," in *Proceedings of the 31st ACM international conference on multimedia*, 2023, pp. 3706–3714.
- [27] C. He, X. Ma, B. B. Zhu, Y. Zeng, H. Hu, X. Bai, H. Jin, and D. Zhang, "Dorpatch: Distributed and occlusion-robust adversarial patch to evade certifiable defenses," in *NDSS*, 2024.
- [28] A. Hore and D. Ziou, "Image quality metrics: Psnr vs. ssim," in *2010 20th international conference on pattern recognition*. IEEE, 2010, pp. 2366–2369.
- [29] L. Liu, J. Chen, H. Wu, G. Li, C. Li, and L. Lin, "Cross-modal collaborative representation learning and a large-scale rgbt benchmark for crowd counting," in *Proceedings of the IEEE/CVF conference on computer vision and pattern recognition*, 2021, pp. 4823–4833.
- [30] Q. Ha, K. Watanabe, T. Karasawa, Y. Ushiku, and T. Harada, "Mfnnet: Towards real-time semantic segmentation for autonomous vehicles with multi-spectral scenes," in *2017 IEEE/RSJ International Conference on Intelligent Robots and Systems (IROS)*. IEEE, 2017, pp. 5108–5115.
- [31] Y. Tian, A. Carballo, R. Li, and K. Takeda, "Road scene graph: A semantic graph-based scene representation dataset for intelligent vehicles," *arXiv preprint arXiv:2011.13588*, 2020.
- [32] X. Wei, Y. Huang, Y. Sun, and J. Yu, "Unified adversarial patch for visible-infrared cross-modal attacks in the physical world," *IEEE Transactions on Pattern Analysis and Machine Intelligence*, vol. 46, no. 4, pp. 2348–2363, 2023.
- [33] X. Yang, W. Zhou, W. Yan, and X. Qian, "Cagnet: Coordinated attention guidance network for rgb-t crowd counting," *Expert Systems with Applications*, vol. 243, p. 122753, 2024.
- [34] W. Kong, Z. Yu, H. Li, and J. Zhang, "Cross-modal misalignment-robust feature fusion for crowd counting," *Engineering Applications of Artificial Intelligence*, vol. 136, p. 108898, 2024.
- [35] G. Zhao, J. Huang, X. Yan, Z. Wang, J. Tang, Y. Ou, X. Hu, and T. Peng, "Open-vocabulary rgb-thermal semantic segmentation," in *European Conference on Computer Vision*. Springer, 2024, pp. 304–320.
- [36] F. Deng, H. Feng, M. Liang, H. Wang, Y. Yang, Y. Gao, J. Chen, J. Hu, X. Guo, and T. L. Lam, "Feagnet: Feature-enhanced attention network for rgb-thermal real-time semantic segmentation," in *2021 IEEE/RSJ international conference on intelligent robots and systems (IROS)*. IEEE, 2021, pp. 4467–4473.
- [37] Y. Wang, G. Li, and Z. Liu, "Sgfnnet: Semantic-guided fusion network for rgb-thermal semantic segmentation," *IEEE Transactions on Circuits and Systems for Video Technology*, vol. 33, no. 12, pp. 7737–7748, 2023.
- [38] Z. Wang, Y. Wu, J. Wang, J. Xu, and W. Shao, "Res2fusion: Infrared and visible image fusion based on dense res2net and double nonlocal attention models," *IEEE Transactions on Instrumentation and Measurement*, vol. 71, pp. 1–12, 2022.
- [39] Z. Wang, J. Wang, Y. Wu, J. Xu, and X. Zhang, "Unfusion: A unified multi-scale densely connected network for infrared and visible image fusion," *IEEE Transactions on Circuits and Systems for Video Technology*, vol. 32, no. 6, pp. 3360–3374, 2021.
- [40] J. Li, J. Jiang, P. Liang, J. Ma, and L. Nie, "Maefuse: Transferring omni features with pretrained masked autoencoders for infrared and visible image fusion via guided training," *IEEE Transactions on Image Processing*, 2025.
- [41] T. O. Hodson, "Root mean square error (rmse) or mean absolute error (mae): When to use them or not," *Geoscientific Model Development Discussions*, vol. 2022, pp. 1–10, 2022.
- [42] S. Pang, H. Huo, X. Yang, J. Li, and X. Liu, "Infrared and visible image fusion based on double fluid pyramids and multi-scale gradient residual block," *Infrared Physics & Technology*, vol. 131, p. 104702, 2023.
- [43] Y. Han, Y. Cai, Y. Cao, and X. Xu, "A new image fusion performance metric based on visual information fidelity," *Information fusion*, vol. 14, no. 2, pp. 127–135, 2013.
- [44] J. Liu, G. Wu, Z. Liu, D. Wang, Z. Jiang, L. Ma, W. Zhong, and X. Fan, "Infrared and visible image fusion: From data compatibility to task adaption," *IEEE Transactions on Pattern Analysis and Machine Intelligence*, 2024.
- [45] Z. Liu, Q. Liu, T. Liu, N. Xu, X. Lin, Y. Wang, and W. Wen, "Feature distillation: Dnn-oriented jpeg compression against adversarial examples," in *2019 IEEE/CVF Conference on Computer Vision and Pattern Recognition (CVPR)*. IEEE, 2019, pp. 860–868.
- [46] S. Gu, P. Yi, T. Zhu, Y. Yao, and W. Wang, "Detecting adversarial examples in deep neural networks using normalizing filters," in *ICAART (2)*, 2019, pp. 164–173.
- [47] B. Li, T. Hu, X. Liu, J. Xie, and P. Yi, "Generalizable poisoning-resistant backdoor detection and removal framework: From dataset perspective," *Pattern Recognition*, p. 112766, 2025.